Langmuir

ARTICLE

pubs.acs.org/Langmuir

Robust Multilayer Thin Films Containing Cationic Thiol-Functionalized Gold Nanorods for Tunable Plasmonic Properties

Ying Bao,[†] Leonid Vigderman,[‡] Eugene R. Zubarev,[‡] and Chaoyang Jiang*[,†]

[†]Department of Chemistry, University of South Dakota, Vermillion, South Dakota 57069, United States

[‡]Department of Chemistry, Rice University, Houston, Texas 77005, United States

ABSTRACT: Gold nanorods have great potential in a variety of applications because of their unique physical properties. In this article, we present the layer-by-layer (LbL) assembly of thin films containing positively charged gold nanorods that are covalently functionalized by cationic thiol molecules. The cationic gold nanorods are uniformly distributed in ultrathin nanocomposite LbL thin films. We studied the collective surface plasmon resonance coupling in the LbL films via UV−visible spectroscopy and evaluated their application in the surface-enhanced Raman scattering detection of rhodamine 6G probe molecules. Furthermore, we successfully manufactured freestanding nanoscale thin films containing multilayers of gold nanorods with a total thickness of less than 50 nm. The surface morphology and their optical and mechanical properties were systematically investigated, and the polycationic gold nanorods were found to play an important role in manipulating the properties of the nanocomposite thin films. Our findings reveal that such nanorods are excellent building blocks for constructing functional LbL films with tunable plasmonic behavior and robust mechanical properties.

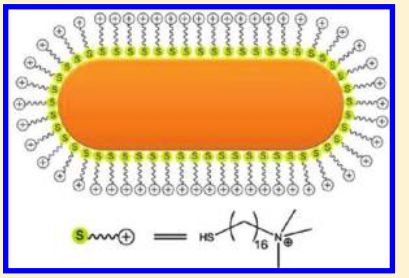

INTRODUCTION

Gold nanostructures and their composite nanomaterials have received much attention during the past decade because of their unique physical and chemical properties and wide applications in biosensing,[1−3] thermal therapy,[4,5] and optics.[6−9] Gold nanorods (Au NRs),[10] with their distinctive 1D structure, have been studied extensively in terms of their syntheses,[11,12] surface modifications,[13−16] optical properties,[17−20] and photothermal therapy.[21−23] Most of these studies are related to two characteristic plasmon bands of Au NRs caused by their localized surface plasmon resonances (LSPRs): a transverse band in the visible region and a longitudinal band in the near-infrared (NIR) region. Previous studies have shown that the longitudinal plasmon band of Au NRs is sensitive to the environment[24] and thus can be significantly impacted by the methods utilized during nanocomposite fabrication. With the rational design of nanoscopic structures, gold nanorod-based composites can precisely tune their plasmonic properties, thus achieving even broader functionalities and applications.

To date, a variety of methods have been utilized to fabricate functional materials from gold nanostructures, such as polymer-mediated assembly,[25−28] template-based assembly,[28−30] interface assembly,[31] and DNA-assisted organization.[32] Liz-Marzán and co-workers prepared Au NR-poly(vinyl alcohol) nanocomposite films by drying a nanorod colloid in the presence of dissolved polymer.[33] Murphy and co-workers modified the gold nanorod surfaces and successfully transferred them from aqueous media to organic solvents, which facilitates the incorporation of nanorods into hydrophobic polymers.[34] Recently, Chen and co-workers reported an approach to assembleing gold nanorods by using block copolymers for encapsulation.[27] Zubarev et al. fabricated bimetallic structures by depositing polycrystalline continuous shells of platinum on the surfaces of Au NRs and subsequently functionalized them with polystyrene chains.[35] Most of these methods require specific surface modification before the assembly processes, and it is still a challenge to incorporate Au NRs into nanocomposite thin films with a well-controlled density and uniform distribution.

However, layer-by-layer (LbL) assembly is a versatile approach to creating nanocomposite thin films with multiple functionalities and designed morphology.[36−38] Multilayer LbL films can be mechanically stable and freely suspended because of strong interactions between multiple layers[38−40] and have been used for a broad range of applications, including superhydrophobic coatings,[41] ultrahard materials,[42] and fuel cells.[43] There are several reports on using LbL assembly to fabricate multilayer films containing Au NRs.[44−46] For example, Tsukruk and his co-workers reported a type of hydrogel LbL films incorporated with gold nanorods, and these films can be used as pH-sensitive optical materials.[47] However, there are still some issues related to their noncovalent coating. First, cetyltrimethylamonium bromide (CTAB), which is an essential surfactant in most gold nanorod syntheses, is involved in dynamic exchange with the free molecules in solution.[48−51] Second, there has to be a certain number of free CTAB molecules in the colloidal solution, which might have a detrimental influence on Au NR deposition and affect the formation of ultrathin films. However, covalently bonded capping agents on the surfaces of gold nanorods not only can significantly stabilize the colloidal gold nanorods but

Received: October 12, 2011
Revised: November 15, 2011
Published: November 22, 2011

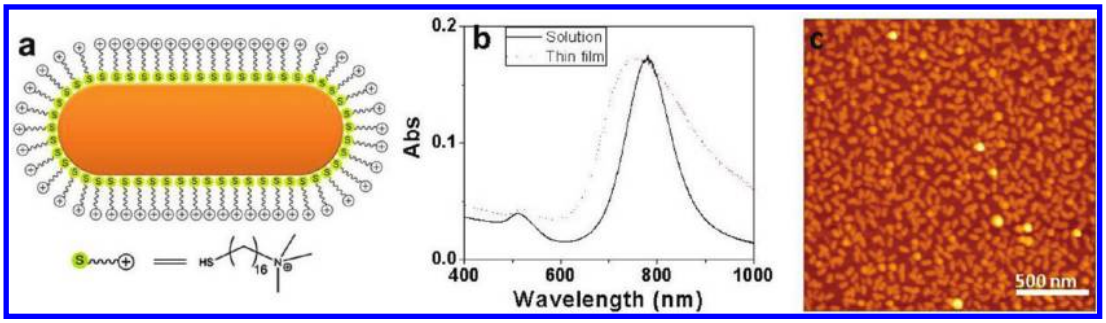

Figure 1. (a) Schematic representation of cationic thiol-functionalized gold nanorods (CT-NRs). (b) UV−vis absorption spectra of CT-NRs in solution and in thin films. (c) AFM image of a CT-NR thin film.

also can promote the integration of hierarchical systems when no free surfactant is present.

Herein, we report the fabrication of functional thin films with covalently functionalized polycationic gold nanorods by using a facile spin-assisted LbL assembly (SA-LbL) and a systematic study of their plasmonic and mechanical properties. These thin films have tunable plasmon resonance bands and show a significant surface-enhanced Raman scattering (SERS) effect. Furthermore, we prepared robust, freely suspended ultrathin nanomembranes containing gold nanorods and have examined their mechanical properties via buckling instability tests. We believe that our approach to assembling gold nanorods into polymeric LbL thin films might provide new possibilities to fabricate novel composite films for potential applications in electronic devices, biosensing, and drug delivery.

EXPERIMENTAL SECTION

Materials and Chemicals. Poly(allylamine hydrochloride) (PAH, MW = 56 000), poly(sodium 4-styrenesulfonate) (PSS, MW = 70 000), and sodium borohydride ($NaBH_4$, 99%) were obtained from Aldrich. Rhodamine 6G (R6G) were purchased from Acros. Nanopure water with a resistivity of 18 MΩ cm was used in all of the experiments. Gold nanorods functionalized with cationic thiol 16-mercaptohexadecyltrimethylammonium bromide were synthesized and fully characterized as described elsewhere.[52] Negatively charged citrate-coated gold nanoparticles (Au NPs, 13 nm in diameter) were prepared according to the well-known citrate reduction method as described in the literature.[53]

LbL Thin Film Fabrication. For thin film fabrication, glass slide substrates were cut to a typical size of 10 × 20 mm^2 and cleaned in a piranha solution (3:1 v/v H_2SO_4/H_2O_2). (***Caution!*** *Piranha solution is extremely dangerous and should be handled very carefully.*) After that, the substrates were rinsed with Nanopure water at least three times and stored in water. The LbL thin films (general formula: $(PAH/PSS)_n$/cationic gold nanorods) were fabricated by the SA-LbL method as described before.[39] All of the procedures were performed in a class 100 softwall clean room. Three types of multilayer thin films containing cationic thiol-coated gold nanorods (CT-NRs) were prepared in this work: gold nanorod thin films composed of a single layer of PAH, PSS, and CT-NRs; gold nanorod−nanoparticle films; and multilayer gold nanorod thin films. For the gold nanorod−nanoparticle films, we have recorded the absorption spectra after adding each gold nanomaterial layer in order to monitor the changes in the surface plasmon resonances (SPRs). Multilayer gold nanorod thin films have a general formula of $[(PAH/PSS)_5/CT\text{-}NRs]_n$, which will be abbreviated as $(5G)_n$, where n is the repeating number of $(PAH/PSS)_5$ and gold nanorod multilayers. To prepare a freestanding thin film, a sacrificial cellulose acetate (CA) layer was first spun on the glass substrate before further deposition.[54] Freestanding LbL thin films can be obtained by dissolving the sacrificial CA layer in acetone. The freestanding LbL films can be lifted from the solution using a variety of substrates, such as glass slides, silicon wafers, and copper grids for further characterization and investigation.

Characterization. We have utilized a variety of microscopic techniques to study the LbL multilayer thin films containing CT-NRs. Optical micrographs were obtained on an Olympus BX41 microscope using a 50× objective (NA = 0.75) and recorded with a 3 megapixel CCD camera. The morphology and thickness of multilayer thin films were measured on a Nano-R^2 atomic force microscope (AFM, Pacific Nanotechnology Inc. Santa Clara, CA) using tapping mode under ambient conditions. Rhodamine 6G solutions with different concentrations were used to evaluate the SERS efficiency of the gold nanorod−nanoparticle thin films. The SERS spectra were acquired on a scanning confocal Raman microscope (Aramis, Horiba Jobin Yvon, Edison, NJ) equipped with a diode-pumped solid-state (DSPP) laser (532 nm) with an intensity of 1.7 mW. SERS spectra were collected with a 50× objective and guided through a Raman filter, a pinhole (500 μm diameter), and a slit (200 μm) into a 460 mm spectrograph. A multichannel thermoelectrically cooled (−70 °C) CCD camera was used to collect the Raman spectra. Transmission electron microscopy (TEM) images of the freestanding multilayer nanomembranes $(5G)_3$ were obtained on a FEI Tecnai TF30 field emission TEM operated at 300 kV. The $(5G)_3$ freestanding films were deposited onto a copper grid and dried overnight before the TEM investigations. The scanning electron microscopy (SEM) study on the gold nanorod−nanoparticle film was conducted on an FEI Quanta 400 SEM after sputtering the sample with 5 nm of gold to increase the surface conductivity.

Mechanical Tests. We followed a well-established method, the buckling instability test, to evaluate the mechanical properties of the freestanding ultrathin multilayer gold nanorod films.[55,56] Soft substrates, poly(dimethylsiloxane) (PDMS) elastomers, were prepared by casting prepolymer Sylgard 185 and its curing agent in a ratio of 10:1 in a glass Petri dish. After careful degassing for 4 h, the PDMS substrates were cured at 70 °C for 2 h. The freestanding LbL thin film was deposited onto a PDMS substrate and was allowed to dry, usually overnight. Buckling patterns were formed by slightly compressing the PDMS (typically less than 2%). We have used an optical microscope to record the buckling images and ImageJ software for data processing. During the calculation of Young's modulus of the LbL thin films, we have assumed that the modulus of the PDMS elastomer is 1.8 MPa, according to the literature report.[57,58]

RESULTS AND DISCUSSION

Gold Nanorod Thin Films. Because of their polycationic monolayer coating, the CT-NRs are stable in pure water and do not contain any free surfactant (Figure 1a). They have intense

extinctions in the visible region due to localized surface plasmon resonances, and these optical properties are sensitive to the nanorods' shape, size, and environment. Figure 1b shows the UV−vis extinction spectra of CT-NRs in aqueous solution (solid line) and their monolayer deposited on a polyelectrolyte multilayer matrix (dashed line). In both spectra, two distinct peaks can be observed at around 515 and 770 nm, which are assigned to the transverse and longitudinal plasmon resonances, respectively.[59−61] Comparing the two spectra in Figure 1b, we found that they have a similar extinction peak at 515 nm (transverse peak), whereas the longitudinal peak of the CT-NR thin film is blue shifted from 780 to 755 nm after deposition onto the PAH/PSS polyelectrolyte matrix. It is known that the longitudinal peak is extremely sensitive to the dielectric constant of the immediate environment. The blue shift could originate from the decrease in the refractive index of the surrounding materials (refractive index from 1.333 of water to almost 1 for CT-NRs on the surface of the polyelectrolyte multilayer).[45,62] Such a blue shift in the longitudinal SPR peak is consistent with a literature report on gold nanorod LbL films.[46] It is noteworthy that the longitudinal peak of the CT-NRs on thin films is broader than that in solution and there are a significant portion of extinctions in the long-wavelength region (800 to 1000 nm). Such broadening and long-wavelength extinction can be explained by the coupling of surface plasmon resonances between gold nanorods as a result of their short inter-rod distance.

The LbL deposition of Au NRs on polyelectrolyte multilayers was studied using atomic force microscopy. As shown in Figure 1c, we deposited a layer of isolated CT-NRs onto the polymer surface with a uniform density and random orientation. The CT-NRs have an apparent diameter (∼15 nm) as obtained from the AFM image analysis. The aspect ratio of ∼2.7 (a result from the TEM study) is consistent with the AFM results considering the dilation effect. In our AFM experiments, we observed that most CT-NRs are well isolated and very little aggregation takes place. The LbL assembly allows for density control of the cationic gold nanorods by tuning the fabricating parameters such as the solution concentration, duration of deposition, and so forth. This data suggests that LbL assembly is a facile method for fabricating nanomaterials containing covalently functionalized cationic gold nanorods in which no free surfactant is present.

Gold Nanorod−Nanoparticle Thin Films. To manipulate the LSPRs of the gold nanorods in the LbL thin films, we fabricated a new type of nanocomposite thin film consisting solely of cationic, covalently functionalized CT-NRs and anionic, citrate-stabilized NPs. We hypothesized that it would be possible to completely replace the traditional polymer electrolytes used in LbL deposition by using highly charged nanoparticles, wherein the NRs would act as polycations and the NPs would act as polyanions. In particular, we were interested in exploring the LSPR coupling between the gold nanorods and nanoparticles, which could play an important role in enhancing the SERS activity. Similar nanohybrid structure-combining nanoparticles with nanorods have been studied by Tsukruk's group, where a silver−gold, core−double-shell nanowire hybrid structure was reported with improved SERS activity.[63] By carrying out multiple LbL deposition steps with alternating cationic NRs and anionic NPs, we were able to construct polymer-free thin films containing solely gold nanostructures. The unique advantage of such a metal−metal structure containing anisotropic gold nanorods is that we can easily tune the LSPR peaks into the NIR region and furthermore have LSPR peaks with a much high intensity in that region, which cannot be achieved with spherical gold particles.

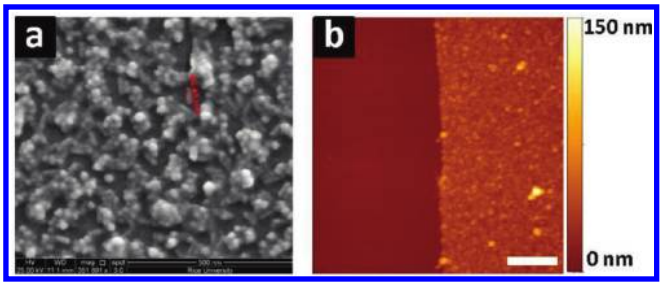

Figure 2. (a) SEM image of a thin film formed from 10 depositions of cationic gold nanorods and anionic gold nanoparticles. (b) AFM image of an edge of the thin film. The scale bar is 2 μm.

Figure 2a shows an SEM micrograph of a gold nanorod−nanoparticle thin film created with a total of 20 depositions of gold nanostructures. A mixture of gold nanorods and gold nanoparticles can be observed from the SEM image. Most of the gold nanoparticles are attached to gold nanorods because of the strong electrostatic interaction between the two oppositely charged species. It should be noted that the nanorod−nanoparticle assembly is not closely packed. The oppositely charged nanostructure can attach laterally with respect to the underlying particle and partially fill the space within the thin films instead of stacking in the vertical direction. This was further confirmed by AFM measurement when the edge of the film was scanned as shown in Figure 2b. The gold nanorod−nanoparticle thin film was quite uniform, and AFM results indicated a low surface roughness of 5.3 nm for a one-bilayer gold nanorod−nanoparticle thin film and 4.3 nm for a 5 bilayer thin film. The trend in surface roughness for such gold a nanorod−nanoparticle thin film is slightly different as compared to that of the $(Fe_3O_4/PAH)_n$ multilayer studied by Möhwald's group.[64] Such a difference can be related to the presence of a polyelectrolyte layer, which plays an important role in film thickness and roughness. We also observed a smooth effect when polyelectrolyte layers were assembled in the LbL films, as discussed below. It is worth noting that the thickness of the thin film was around 30 ± 5 nm, a value that was much lower than the initial prediction with a close-packing model. AFM thickness measurements supported the idea of lateral aggregation during the consecutive deposition of oppositely charged gold nanostructures.

The increasing aggregation of nanorods and nanoparticles in the thin films is expected to influence their plasmonic properties strongly. We monitored the LSPR properties of the gold nanorod−nanoparticle thin films by examining their UV−visible absorption spectra during the LbL assembly process. A series of UV−vis spectra are shown in Figure 3a. Two distinctive SPR peaks can be clearly observed from each of these spectra, and the change in the position and intensity of these peaks is depicted in the plot shown in Figure 3b. As the number of depositions increases, a red shift in the SPR peaks can be clearly observed, with the transverse band shifting from 515 to 613 nm and the longitudinal band shifting from 767 to 925 nm. It is interesting that the deposition of gold nanorods leads to a significant red shift of primarily the longitudinal band whereas the deposition of nanoparticles red shifts the transverse band. This can be explained by the different origination of these two LSPR peaks. The longitudinal peak of Au NRs is more sensitive to the length of the gold NRs. The addition of gold nanorods can

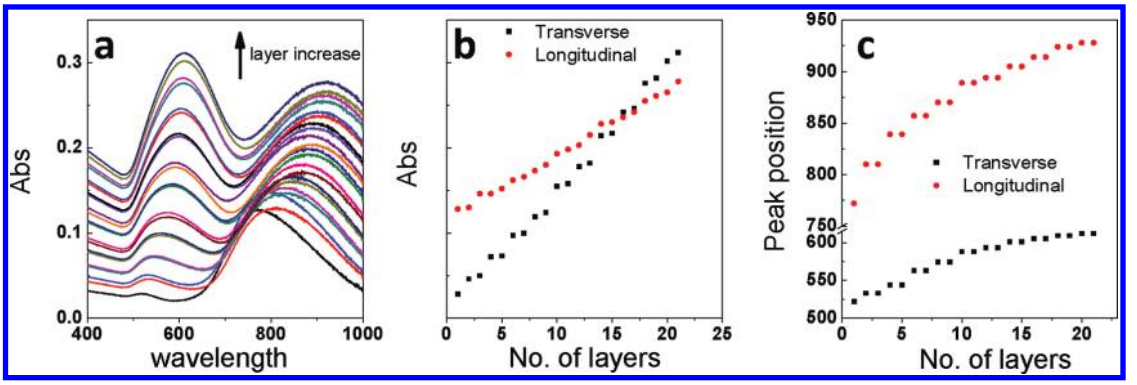

Figure 3. (a) UV−vis absorption spectra of the LbL film consisting of increasing depositions of gold nanorods−nanoparticles up to 10. (b) Intensity changes in the longitudinal peak and transverse peak with increasing deposition number. (c) Position changes in the longitudinal peak and transverse peak as a function of the change in the deposition number.

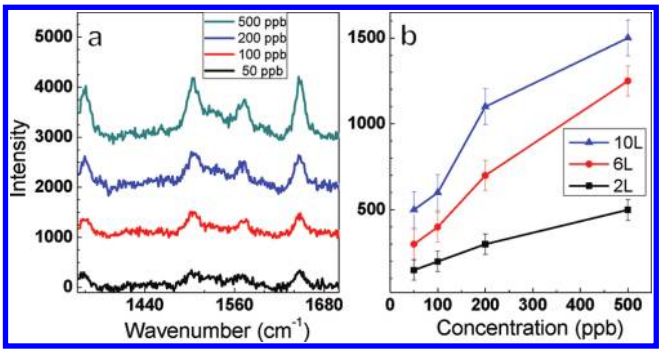

Figure 4. (a) SERS spectra of concentration as a function of a 6 bilayer gold nanorod−nanoparticle thin film. (b) Plots of SERS intensity vs different concentration of 2, 6, and 10 bilayers.

have a more significant effect on the length of the gold nanostructures as compared to the addition of gold nanoparticles. Therefore, additions of Au NRs will significantly red shift the longitudinal band in the extinction spectra. Similarly, gold nanoparticles will change the local environment sufficiently, resulting in strong coupling with the transverse band. Our work clearly demonstrated that the optical properties of a composite thin film can be controlled by tuning the aggregation of both Au NRs and NPs through the SA-LbL deposition process.

We further explored the SERS enhancement on the gold nanorod−nanoparticle thin films by using rhodamine 6G (R6G) as a probe molecule. It has been known that a strong SERS enhancement will be induced by the formation of metal nanoparticle assemblies.[65] Thus, gold nanorod−nanoparticle thin films are expected to have a high SERS enhancement for molecular sensing applications. We examined the SERS properties of our film by measuring the SERS signal intensity for R6G solutions at concentrations of 50, 100, 200, and 500 ppb. Figure 4a shows the SERS spectra of R6G adsorbed on the gold nanorod−nanoparticle thin film (12 CT-NR/citrate NP deposition steps). From the spectrum, one can see that the R6G Raman peaks are located at 1357, 1508, 1572, and 1647 cm^{-1}, which are assigned to C−H in-plane bending, C−O−C stretching, and aromatic C−C stretching, respectively.[66] As expected, increased R6G concentrations led to an increase in the intensity of the SERS peaks measured. Even for an R6G solution with a concentration of 50 ppb, the R6G Raman peaks at 1647 cm^{-1} can be clearly detected with a signal-to-noise ratio that is greater than 3.7. Although it is difficult to estimate the SERS enhancement factor (EF) directly for R6G in our measurements, the ability to detect a 50 ppb R6G solution indicates the excellent SERS activity of the gold nanorod−nanoparticle thin films.[67]

Figure 4b compares the intensities of the 1508 cm^{-1} Raman peak on three thin films with different numbers of NR−NP depositions. The intensities of the SERS peaks are quite reproducible, and the standard derivations of the intensities of the Raman peaks are also shown in the figure as a function of the noise of the experiments. From the plot, we can see that thin films with large number of depositions have significantly better SERS enhancement than those with less depositions. We hypothesize that increasing aggregation between gold nanorods and nanoparticles occurs with more rounds of deposition, leading to an increased number of SERS-active hot spots at the various nanoparticle junctions as as result of the strong electromagnetic field enhancement at these points.[68−70]

Multilayer Gold Nanorod Thin Films. In addition to gold nanorod thin films and gold nanorod−nanoparticle thin films, we have fabricated multilayer gold nanorod thin films, $(5G)_n$, where layers of CT-NRs are sandwiched in a polyelectrolyte multilayer matrix. We have systematically studied the microstructures and optical properties of such gold nanorod multilayer thin films.

We first conducted AFM measurements to characterize the morphology and thickness of $(5G)_n$ multilayer thin films. Figure 5 shows the AFM topographies of $(5G)_n$ films as more layers are deposited. Profile scans for the AFM images are also shown in Figure 5. For all three films, gold nanorods are uniformly distributed with random lateral orientation in the polymeric multilayers. With an increasing number of (5G) repeat units, a higher density of CT-NRs can be observed in the AFM images and the thickness of the $(5G)_n$ multilayers also increases. We obtained thicknesses of 20.1 ± 3.9, 31.2 ± 3.5, and 49.2 ± 6.1 nm for multilayers of $(5G)_1$, $(5G)_2$, and $(5G)_3$, respectively. It is reasonable to expect such a nonlinear increase in the film thickness of $(5G)_n$ multilayers because the additional deposition of polyelectrolyte layers and gold nanorods occurs on the rough surfaces of nanocomposite thin films instead of on a smooth surface. We would expect to see a decrease in the surface roughness due to the continuous multilayer deposition (a smoothing effect). The smoothing effect of multilayer deposition on nanoscale particles was also confirmed by Möhwald's group in their recent article.[71] Such an assumption is consistent with the roughness measurements of the LbL films that were conducted with the AFM

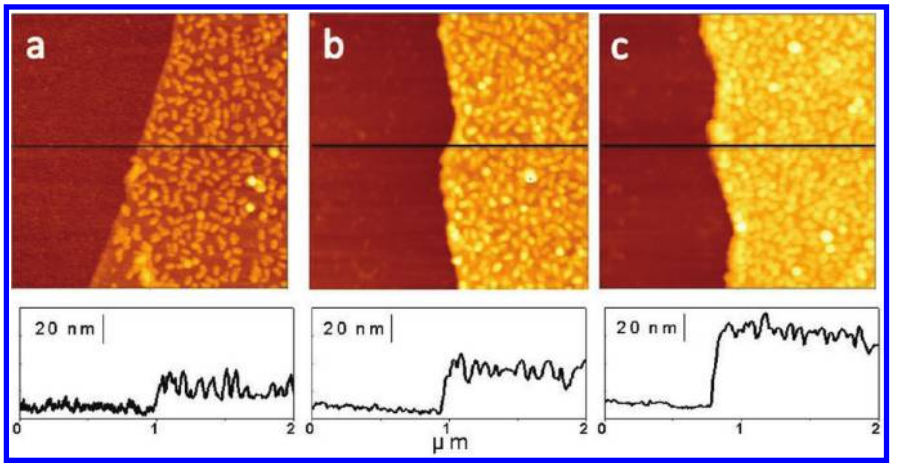

Figure 5. AFM images ($2 \times 2\,\mu m^2$) and line profiles of (a) $(5G)_1$, (b) $(5G)_2$, and (c) $(5G)_3$ LbL thin films on silicon substrates. These AFM images are processed on the same z scale for easy comparison.

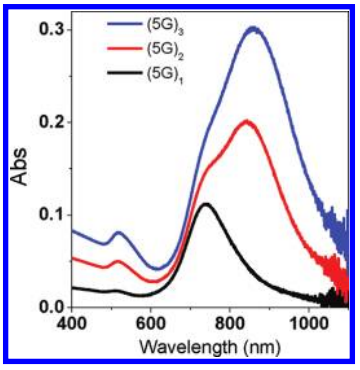

Figure 6. UV−vis spectra of $(5G)_1$, $(5G)_2$, and $(5G)_3$ thin films.

software. We observed a slight decrease in the surface roughness from 6.1 nm for $(5G)_1$ films to 5.8 nm for $(5G)_3$ thin films.

The UV−vis extinction spectra of the gold nanorod multilayer films change dramatically with an increasing number of nanorod layers. The extinction spectra of $(5G)_1$, $(5G)_2$, and $(5G)_3$ thin films were obtained as shown in Figure 6. The transverse and longitudinal surface plasmon bands of the $(5G)_1$ film were located at 516 and 740 nm, respectively. We decreased the density of NRs deposited in a single layer in an effort to decrease intralayer plasmon coupling so that interlayer plasmon coupling could be more clearly observed. Indeed, the $(5G)_1$ absorbance shows almost no shift in the LSPR as compared to free CT-NRs, indicating that little coupling is occurring between NRs in a single layer. As more layers of polyelectrolyte and CT-NRs are deposited, the spectrum shows a steady increase in intensity and a new absorption band appears at around 843 nm. This new band is believed to be attributed to the interlayer LSPR coupling between gold nanorods, similar to previous reports on multilayer LbL films of gold nanoparticles.[53,72] For the $(5G)_3$ films, the intensity of the 843 nm peak, as well as its relative height compared to the regular LSPR peak, is much larger than those of $(5G)_2$, indicating more interlayer coupling between gold nanorods.

We have further fabricated freestanding gold nanorod LbL films and explored their microstructures and mechanical properties. As far as we know, this is the first report on fabricating robust freestanding ultrathin LbL films containing gold nanorods. The schematic representation of the $(5G)_3$ freestanding film is showing in Figure 7a. A sacrificial layer of cellulose acetate was spun onto glass or silicon substrates before the LbL deposition of polyelectrolytes and gold nanorods, followed by the dissolution of the sacrificial layer with acetone to prepare a freestanding film. The polyelectrolyte layer is quite smooth initially,[73] though the deposition of gold nanorods should increase the surface roughness of the multilayer thin films. Figure 7b,c shows the AFM topography of the front side of the freestanding thin film, which has gold nanorods on its surface, and the back side of freestanding film (polymer surface), respectively. The morphologies of these two surfaces are quite different. Gold nanorods can be clearly observed on the front side of the freestanding film. From the AFM images, we can see that the surface roughness of the back side is much lower than that of the front side of the LbL film, with an rms roughness of 3.0 nm compared to 5.7 nm.

The freestanding $(5G)_3$ LbL films are mechanically robust, and the high density of covalently functionalized gold nanorods and the interaction between the polymers and cationic CT-NRs play key roles in the nanocomposite stability. Importantly, we were unsuccessful in our attempts to use conventional CTAB-coated gold nanorods to fabricate freestanding LbL films, which indicates the importance of the covalent functionalization of gold nanorods and the absence of free surfactant. Figure 8a shows an optical image of a $(5G)_3$ thin film that is freely suspended on a copper grid with openings of as large as 50 μm. The films are optically uniform across several hundred micrometers, indicating excellent control of the gold nanorod dispersion during the LbL process. This thin film with a total thickness of less than 100 nm is very stable for at least several months and can withstand the high-vacuum condition necessary for TEM imaging. The TEM micrograph of the freestanding $(5G)_3$ film shown in Figure 8b clearly demonstrates the uniform distribution of gold nanorods throughout the film. The higher-magnification inset in Figure 8b validates the uniform distribution of individual NRs in the film by confirming that there are no large clusters or aggregates of nanorods in the film. The size and shape of gold nanorods in the film match those of free NRs, confirming that the deposition process has no effect on their morphology. On the basis of the particle density from the TEM results, we calculated that the area surface coverage of the gold nanorods is about $30.4 \pm 2.8\%$ in the thin films. Considering that the freestanding thin films are 49 nm

dx.doi.org/10.1021/la203993m |*Langmuir* 2012, 28, 923–930

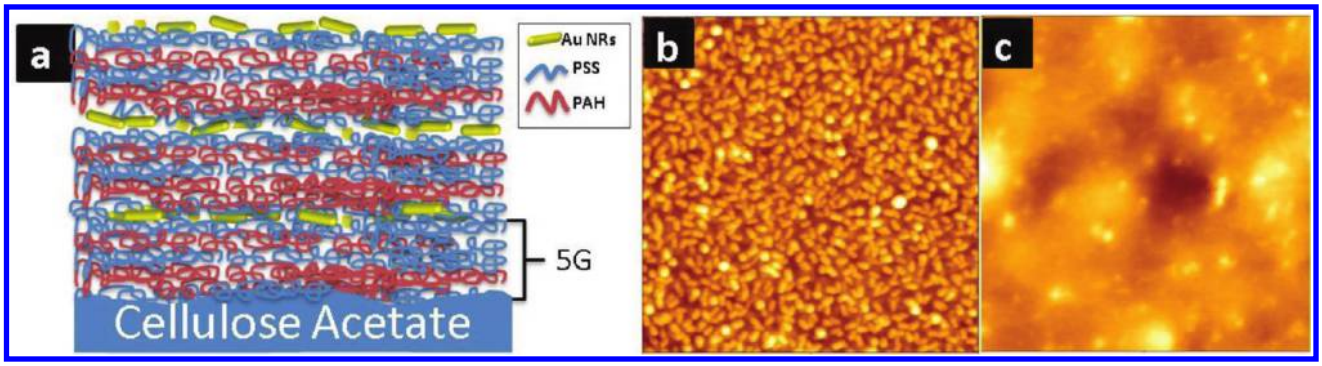

Figure 7. (a) Schematic representation of a $(5G)_3$ freestanding thin film on top of a cellulose acetate sacrificial layer. (b, c) AFM topographies of the front side and the back side of a $(5G)_3$ freestanding thin film, respectively. Image size: $2 \times 2\ \mu m^2$.

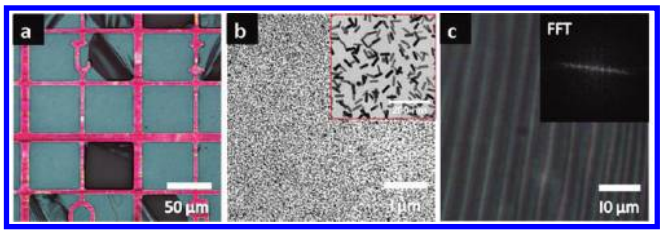

Figure 8. (a) Optical image of a freestanding film deposited on a copper grid. (b) TEM images of CT-NRs uniformly distributed in the film. (Inset) High-magnification image of gold nanorods. (c) Optical image of the buckling of a PDMS-supported $(5G)_3$ freestanding film. (Inset) FFT image of the buckling pattern.

in height, we calculated the volume fraction of CT-NRs in the $(5G)_3$ thin film to be about $5.8 \pm 0.5\%$.

A quantitative study of the mechanical properties of the films was conducted by applying the buckling instability test to $(5G)_3$ LbL films. The samples for buckling tests were prepared by transferring $(5G)_3$ freestanding films onto PDMS substrates. Buckling can be induced by applying lateral compression to the elastomeric substrate. The resulting patterns of deformation were recorded with an optical microscope as shown in Figure 8c. A buckling wavelength (λ) of 2.16 μm and their fast Fourier transform (FFT) patterns (inset of Figure 8c) were measured from the optical images. Young's modulus (E) of the multilayer LbL films can be calculated with the following equation

$$E_f = 3E_s\left(\frac{\lambda}{2\pi d}\right)^3\frac{(1-\nu_f^2)}{(1-\nu_s^2)}$$

where ν is Poisson's ratio, subscripts s and f refer to the substrate and film, respectively, d is the film thickness, and E_s is Young's modulus of the PDMS substrate (assume 1.8 MPa according to the literature).[57,58] From this analysis, we calculated the elastic modulus of the $(5G)_3$ thin film to be $E_f = 2.2$ GPa. Compared to the elastic modulus of the 9G9 multilayer thin film that is about ; 8 ± 3.5 GPa, as reported previously,[40] the $(5G)_3$ thin film has a lower elastic value. This can be attributed to the lower nanorod density in $(5G)_3$ films compared to that of gold nanoparticles in the 9G9 LbL film. Even the density of gold nanorods is low, and the $(5G)_3$ thin film is still relatively robust and mechanically stable.

The robust mechanical properties of the freestanding LbL multilayer thin films can be attributed to the gold nanorods contained in the nanomembranes, as demonstrated by theoretical calculations of the mechanical properties of the composite material. Here we used Halpin−Tsai equations to estimate the elastic modulus of the LbL Au NR thin films. The Halpin−Tsai model is a mathematical model for calculating the elastic modulus of reinforced composite materials based on the size and orientation of the fillers and the mechanical properties of the filler and matrix.[74] The elastic modulus of the inorganic nanoscale filler, gold nanorods, (16 GPa) will be used in our calculation because it has been reported that wet-chemistry-synthesized gold nanorods have a 5-fold smaller Young's modulus than does bulk gold (79 GPa).[75] Considering the volume fraction of the gold nanorods in the composite thin films obtained from the microstructural analyses, we made a rough estimation of the elastic modulus of the thin film to be about 2.3 GPa, which is consistent with our buckling experiments. It is worth noting that Young's modulus of $(5G)_3$ films is much lower than those of LbL films with silver nanowires.[58] We believe that this can be due to the relatively short length of the gold nanorods as compared to the micrometers-long silver nanowires. Because the gold nanorods are less than 50 nm in length, there is much less chance for polyelectrolyte to bridge neighboring gold nanorods, thus resulting in inefficient transfer of the mechanical load onto gold nanorods. Even with this low elastic modulus, the composite $(5G)_3$ multilayer thin films are still mechanically stable, which can be attributed to the strong interaction between the anionic polymers and the cationic, covalently functionalized gold nanorods.

CONCLUSIONS

We reported the fabrication and characterization of ultrathin LbL films with covalently functionalized cationic gold nanorods. Because of the covalent attachment of the positively charged thiol, it was possible to carry out the LbL assembly of gold nanorods into functional composite thin films. Facile spin-assisted LbL assembly was applied to the fabrication of the nanocomposite films containing uniformly distributed gold nanorods. Collective LSPR coupling between gold nanorods, as well as gold nanoparticles, allows for an easy manipulation of the optical properties of the nanocomposite thin films. Gold nanorods in LbL films have demonstrated strong SERS activity in the Raman detection of rhodamine 6G. Robust freestanding nanomembranes with gold nanorods have been demonstrated in our work, and their optical and mechanical properties have been explored. The covalently functionalized gold nanorods in the

LbL films play a key role in these unusual optical and mechanical properties. We believe that our approach of assembling gold nanorods into LbL films might provide new possibilities for fabricating multifunctional nanomembranes for potential applications in advanced biosensing, electronic devices, and drug delivery.

AUTHOR INFORMATION

Corresponding Author

*E-mail: chaoyang.jiang@usd.edu.

ACKNOWLEDGMENT

This research was supported by the NSF (EPS-0903804 and DGE-0903685), NASA (cooperative agreement number NNX10AN34A), and the state of South Dakota. TEM work was conducted on the instrument funded by the NSF CHE-0840507 grant. We are grateful to Dr. C. Lin at the University of South Dakota for his help with TEM measurements. Y.B. is thankful for partial support from the Sigma Xi Grant-in-Aid of Research program. E.R.Z. acknowledges the financial support provided by the NSF (DMR-0547399 and DMR-1105878) and the Welch Foundation (C-1703).

REFERENCES

(1) Tabakman, S. M.; Chen, Z.; Casalongue, H. S.; Wang, H.; Dai, H. *Small* **2011**, *7*, 499–505.
(2) Haes, A.; Stuart, D.; Nie, S.; Van Duyne, R. *J. Fluoresc.* **2004**, *14*, 355–367.
(3) Castellana, E. T.; Gamez, R. C.; Russell, D. H. *J. Am. Chem. Soc.* **2011**, *133*, 4182–4185.
(4) Choi, W. I.; Kim, J.-Y.; Kang, C.; Byeon, C. C.; Kim, Y. H.; Tae, G. *ACS Nano* **2011**, *5*, 1995–2003.
(5) Hirsch, L. R.; Stafford, R. J.; Bankson, J. A.; Sershen, S. R.; Rivera, B.; Price, R. E.; Hazle, J. D.; Halas, N. J.; West, J. L. *Proc. Natl. Acad. Sci. U.S.A.* **2003**, *100*, 13549–13554.
(6) El-Sayed, M. A. *Acc. Chem. Res.* **2001**, *34*, 257–264.
(7) Murphy, C. J.; Gole, A. M.; Hunyadi, S. E.; Orendorff, C. J. *Inorg. Chem.* **2006**, *45*, 7544–7554.
(8) Zeng, J.; Huang, J.; Lu, W.; Wang, X.; Wang, B.; Zhang, S.; Hou, J. *Adv. Mater.* **2007**, *19*, 2172–2176.
(9) Paudel, H. P.; Zhong, L.; Bayat, K.; Baroughi, M. F.; Smith, S.; Lin, C.; Jiang, C.; Berry, M. T.; May, P. S. *J. Phys. Chem. C* **2011**, *115*, 19028–19036.
(10) Pérez-Juste, J.; Pastoriza-Santos, I.; Liz-Marzán, L. M.; Mulvaney, P. *Coordin. Chem. Rev.* **2005**, *249*, 1870–1901.
(11) Martin, C. R. *Science* **1994**, *266*, 1961–1966.
(12) Martin, C. R. *Chem. Mater.* **1996**, *8*, 1739–1746.
(13) Gole, A.; Murphy, C. J. *Langmuir* **2005**, *21*, 10756–10762.
(14) Pramod, P.; Joseph, S. T. S.; Thomas, K. G. *J. Am. Chem. Soc.* **2007**, *129*, 6712–6713.
(15) Shibu Joseph, S. T.; Ipe, B. I.; Pramod, P.; Thomas, K. G. *J. Phys. Chem. B* **2005**, *110*, 150–157.
(16) Dai, Q.; Worden, J. G.; Trullinger, J.; Huo, Q. *J. Am. Chem. Soc.* **2005**, *127*, 8008–8009.
(17) Stone, J. W.; Sisco, P. N.; Goldsmith, E. C.; Baxter, S. C.; Murphy, C. J. *Nano Lett.* **2006**, *7*, 116–119.
(18) Deeb, C.; Zhou, X. A.; Gerard, D.; Bouhelier, A.; Jain, P. K.; Plain, J.; Soppera, O.; Royer, P.; Bachelott, R. *J. Phys. Chem. Lett.* **2011**, *2*, 7–11.
(19) Wang, L. M.; Li, Y. F.; Zhou, L. J.; Liu, Y.; Meng, L.; Zhang, K.; Wu, X. C.; Zhang, L. L.; Li, B.; Chen, C. Y. *Anal. Bioanal. Chem.* **2010**, *396*, 1105–1114.
(20) Alvarez-Puebla, R. A.; Agarwal, A.; Manna, P.; Khanal, B. P.; Aldeanueva-Potel, P.; Carbo-Argibay, E.; Pazos-Perez, N.; Vigderman, L.; Zubarev, E. R.; Kotov, N. A.; Liz-Marzan, L. M. *Proc. Natl. Acad. Sci. U.S.A.* **2011**, *108*, 8157–8161.
(21) Jang, B.; Park, J. Y.; Tung, C. H.; Kim, I. H.; Choi, Y. *ACS Nano* **2011**, *5*, 1086–1094.
(22) Hafner, J. H.; Liao, H. W. *Chem. Mater.* **2005**, *17*, 4636–4641.
(23) Tee, G.; Choi, W. I.; Kim, J. Y.; Kang, C.; Byeon, C. C.; Kim, Y. H. *ACS Nano* **2011**, *5*, 1995–2003.
(24) Murphy, C. J.; Gole, A. M.; Hunyadi, S. E.; Stone, J. W.; Sisco, P. N.; Alkilany, A.; Kinard, B. E.; Hankins, P. *Chem. Commun.* **2008**, 544–557.
(25) Srivastava, S.; Frankamp, B. L.; Rotello, V. M. *Chem. Mater.* **2005**, *17*, 487–490.
(26) Chen, G.; Wang, Y.; Yang, M.; Xu, J.; Goh, S. J.; Pan, M.; Chen, H. *J. Am. Chem. Soc.* **2010**, *132*, 3644–3645.
(27) Chen, T.; Wang, H.; Chen, G.; Wang, Y.; Feng, Y.; Teo, W. S.; Wu, T.; Chen, H. *ACS Nano* **2010**, *4*, 3087–3094.
(28) Lee, C. H.; Tian, L.; Abbas, A.; Kattumenu, R.; Singamaneni, S. *Nanotechnology* **2011**, *22*, 275311.
(29) Wang, L.; Luo, J.; Schadt, M. J.; Zhong, C.-J. *Langmuir* **2009**, *26*, 618–632.
(30) Zubarev, E. R.; Khanal, B. P. *Angew. Chem., Int. Ed.* **2007**, *46*, 2195–2198.
(31) Cheng, L.; Liu, A.; Peng, S.; Duan, H. *ACS Nano* **2010**, *4*, 6098–6104.
(32) Mirkin, C. A.; Letsinger, R. L.; Mucic, R. C.; Storhoff, J. J. *Nature* **1996**, *382*, 607–609.
(33) Perez-Juste, J.; Rodriguez-Gonzalez, B.; Mulvaney, P.; Liz-Marzan, L. M. *Adv. Funct. Mater.* **2005**, *15*, 1065–1071.
(34) Alkilany, A. M.; Thompson, L. B.; Murphy, C. J. *ACS Appl. Mater. Interfaces* **2010**, *2*, 3417–3421.
(35) Khanal, B. P.; Zubarev, E. R. *Angew. Chem., Int. Ed.* **2009**, *48*, 6888–6891.
(36) Decher, G. *Science* **1997**, *277*, 1232–1237.
(37) Hammond, P. T. *Adv. Mater.* **2004**, *16*, 1271–1293.
(38) Jiang, C. Y.; Tsukruk, V. V. *Adv. Mater.* **2006**, *18*, 829–840.
(39) Jiang, C. Y.; Markutsya, S.; Tsukruk, V. V. *Adv. Mater.* **2004**, *16*, 157–161.
(40) Jiang, C. Y.; Markutsya, S.; Pikus, Y.; Tsukruk, V. V. *Nat. Mater.* **2004**, *3*, 721–728.
(41) Zhai, L.; Cebeci, F. C.; Cohen, R. E.; Rubner, M. F. *Nano Lett.* **2004**, *4*, 1349–1353.
(42) Tang, Z. Y.; Kotov, N. A.; Magonov, S.; Ozturk, B. *Nat. Mater.* **2003**, *2*, 413–418.
(43) Lutkenhaus, J. L.; Hammond, P. T. *Soft Matter* **2007**, *3*, 804–816.
(44) Gole, A.; Murphy, C. J. *Chem. Mater.* **2005**, *17*, 1325–1330.
(45) Hu, X. G.; Cheng, W. L.; Wang, T.; Wang, Y. L.; Wang, E. K.; Dong, S. J. *J. Phys. Chem. B* **2005**, *109*, 19385–19389.
(46) Vial, S.; Pastoriza-Santos, I.; Perez-Juste, J.; Liz-Marzan, L. M. *Langmuir* **2007**, *23*, 4606–4611.
(47) Kozlovskaya, V.; Kharlampieva, E.; Khanal, B. P.; Manna, P.; Zubarev, E. R.; Tsukruk, V. V. *Chem. Mater.* **2008**, *20*, 7474–7485.
(48) Connor, E. E.; Mwamuka, J.; Gole, A.; Murphy, C. J.; Wyatt, M. D. *Small* **2005**, *1*, 325–327.
(49) Takahashi, H.; Niidome, Y.; Niidome, T.; Kaneko, K.; Kawasaki, H.; Yamada, S. *Langmuir* **2005**, *22*, 2–5.
(50) Warheit, D. B. *Nano Lett.* **2010**, *10*, 4777–4782.
(51) Mirska, D.; Schirmer, K.; Funari, S. S.; Langner, A.; Dobner, B.; Brezesinski, G. *Colloids Surf., B* **2005**, *40*, 51–59.
(52) Vigderman, L.; Manna, P.; Zubarev, E. R., *Angew. Chem., Int. Ed.* **2012**, DOI: 10.1002/anie.201107304.
(53) Jiang, C.; Markutsya, S.; Tsukruk, V. V. *Langmuir* **2004**, *20*, 882–890.
(54) Kotov, N. A.; Mamedov, A. A. *Langmuir* **2000**, *16*, 5530–5533.
(55) Stafford, C. M.; Harrison, C.; Beers, K. L.; Karim, A.; Amis, E. J.; VanLandingham, M. R.; Kim, H.-C.; Volksen, W.; Miller, R. D.; Simonyi, E. E. *Nat. Mater.* **2004**, *3*, 545–550.

(56) Jiang, C.; Singamaneni, S.; Merrick, E.; Tsukruk, V. V. *Nano Lett.* **2006**, *6*, 2254–2259.
(57) Lee, I.; Hendricks, T. R. *Nano Lett.* **2007**, *7*, 372–379.
(58) Gunawidjaja, R.; Jiang, C. Y.; Peleshanko, S.; Ornatska, M.; Singamaneni, S.; Tsukruk, V. V. *Adv. Funct. Mater.* **2006**, *16*, 2024–2034.
(59) Orendorff, C. J.; Gearheart, L.; Jana, N. R.; Murphy, C. J. *Phys. Chem. Chem. Phys.* **2006**, *8*, 165–170.
(60) Orendorff, C. J.; Gole, A.; Sau, T. K.; Murphy, C. J. *Anal. Chem.* **2005**, *77*, 3261–3266.
(61) Nikoobakht, B.; Wang, J.; El-Sayed, M. A. *Chem. Phys. Lett.* **2002**, *366*, 17–23.
(62) Nikoobakht, B.; El-Sayed, M. A. *J. Phys. Chem. A* **2003**, *107*, 3372–3378.
(63) Gunawidjaja, R.; Peleshanko, S.; Ko, H.; Tsukruk, V. V. *Adv. Mater.* **2008**, *20*, 1544–1549.
(64) Yashchenok, A. M.; Gorin, D. A.; Badylevich, M.; Serdobintsev, A. A.; Bedard, M.; Fedorenko, Y. G.; Khomutov, G. B.; Grigoriev, D. O.; Möhwald, H. *Phys. Chem. Chem. Phys.* **2010**, *12*, 10469–10475.
(65) Lu, Z.; Goebl, J.; Ge, J.; Yin, Y. *J. Mater. Chem.* **2009**, *19*, 4597–4602.
(66) Michaels, A. M.; Nirmal, M.; Brus, L. E. *J. Am. Chem. Soc.* **1999**, *121*, 9932–9939.
(67) Tao, A.; Kim, F.; Hess, C.; Goldberger, J.; He, R. R.; Sun, Y. G.; Xia, Y. N.; Yang, P. D. *Nano Lett.* **2003**, *3*, 1229–1233.
(68) Kho, K. W.; Shen, Z. X.; Zeng, H. C.; Soo, K. C.; Olivo, M. *Anal. Chem.* **2005**, *77*, 7462–7471.
(69) Khan, I.; Cunningham, D.; Littleford, R. E.; Graham, D.; Smith, W. E.; McComb, D. W. *Anal. Chem.* **2005**, *78*, 224–230.
(70) Maxwell, D. J.; Emory, S. R.; Nie, S. *Chem. Mater.* **2001**, *13*, 1082–1088.
(71) Grigoriev, D.; Gorin, D.; Sukhorukov, G. B.; Yashchenok, A.; Maltseva, E.; Möhwald, H. *Langmuir* **2007**, *23*, 12388–12396.
(72) Yun, S.; Oh, M. K.; Kim, S. K.; Park, S. *J. Phys. Chem. C* **2009**, *113*, 13551–13557.
(73) Bao, Y.; Luu, Q. A. N.; Lin, C.; Schloss, J. M.; May, P. S.; Jiang, C. *J. Mater. Chem.* **2010**, *20*, 8356–8361.
(74) Affdl, J. C. H.; Kardos, J. L. *Polym. Eng. Sci.* **1976**, *16*, 344–352.
(75) Hartland, G. V.; Hu, M.; Hillyard, P.; Kosel, T.; Perez-Juste, J.; Mulvaney, P. *Nano Lett.* **2004**, *4*, 2493–2497.